Available online at www.sciencedirect.com
SCIENCE DIRECT®
Chemical Physics Letters 371 (2003) 157–163
CHEMICAL PHYSICS LETTERS
www.elsevier.com/locate/cplett

Electronic states in 2-aminopurine revealed by ultrafast transient absorption and target analysis

Olaf F.A. Larsen [a,*], Ivo H.M. van Stokkum [a], Marie-Louise Groot [a], John T.M. Kennis [a], Rienk van Grondelle [a], Herbert van Amerongen [b]

[a] *Division of Physics and Astronomy, Faculty of Sciences, Vrije Universiteit Amsterdam, De Boelelaan 1081, 1081 HV Amsterdam, Netherlands*
[b] *Laboratory of Biophysics, Department of Agrotechnology and Food Sciences, Dreijenlaan 3, 6703 HA Wageningen, Netherlands*

Received 18 November 2002; in final form 27 January 2003

Abstract

Subpicosecond polarized transient-absorption measurements on the fluorescent adenine analogue 2-aminopurine have been performed in the wavelength region from 320 to 690 nm. Global target analysis of the data reveals structural heterogeneity of the chromophore in the excited state. Two distinct states with remarkably different spectroscopic properties were resolved. One state does show stimulated emission, whereas the other state does not and exposes a very long excited-state lifetime.

1. Introduction

The study of the dynamical and charge-transfer properties of DNA is a research area of intense interest [1–4]. For performing (time-resolved) fluorescence spectroscopy, the use of extrinsic probes is a prerequisite because of the very low fluorescence quantum yield of the natural nucleic acids [5]. The adenine analogue 2-aminopurine (2AP) is a widely used probe for these purposes [6–9], because of its high fluorescence quantum yield (0.66), its red-shifted absorption allowing selective excitation, and its property to build into the DNA B-helix without significant structural disturbance [10,11]. Introduction of 2AP into DNA causes a large reduction of the fluorescence quantum yield, which is attributed to stacking interactions with the neighboring bases possibly causing charge transfer processes [8].

Two different tautomeric states of 2AP are known; the 9-H and 7-H tautomers that have a proton at, respectively, nitrogen number 9 and 7. Both calculations and experiments show that 2AP in the ground state mainly exists as the 9-H tautomer [10,12]. However, recent experiments and calculations suggest that the 7-H tautomer might be present in significant amounts upon excitation [13,14].

A better understanding of the 2AP quenching mechanism and thus of the dynamical and charge-

* Corresponding author. Present address: Foundation for Fundamental Research on Matter Institute for Atomic and Molecular Physics, Kruislaan 407, 1098 SJ Amsterdam, The Netherlands.
E-mail address: olaf_larsen@hotmail.com (O.F.A. Larsen).

0009-2614/03/$ - see front matter
doi:10.1016/S0009-2614(03)00212-4

transfer properties of DNA requires a thorough knowledge of the underlying photophysics of isolated 2AP as compared to 2AP incorporated in DNA. In this study we have therefore measured the transient-absorption spectra of 2AP with subpicosecond time resolution.

2. Experimental section

2.1. Chemicals

2AP (Sigma Aldrich, Zwijndrecht) with a purity of >99% was dissolved in a 20 mM Na_2HPO_4/NaH_2PO_4, 0.1M NaCl, pH 7.0, buffer, and continuously flowed during the experiment to avoid photodecomposition.

2.2. Subpicosecond transient-absorption setup

The setup consists of a 1-kHz Ti:sapphire amplifier and non-collinear optical parametric amplifier (NOPA) system as described in more detail elsewhere [15]. Briefly, femtosecond (pump) excitation-pulses centered at 309 nm were generated by frequency mixing of the 506 nm output of the NOPA with 800 nm pulses. The time evolution of the excited-state dynamics was subsequently monitored using a white-light (probe) pulse, resulting in an instrument response of ~600 fs FWHM. Transient-absorption spectra (absorption difference of the white-light with and without pump pulse) were monitored. Four different wavelength intervals were probed (each spanning ~120 nm and all together ranging from ~320 to ~690 nm), which were simultaneously analyzed. The white-light continuum was generated using a CaF_2 crystal, which was continuously translated to avoid burning. No significant signal of hydrated electrons from 2AP was observed, which are known to be formed when very high excitation densities are used [16]. Both anisotropic (parallel and perpendicularly polarized) as well as isotropic signals were recorded.

3. Results

In Fig. 1, several representative transient-absorption traces at different wavelengths are shown.

It is immediately clear from the data that the polarization behavior of 2AP changes dramatically with the probe wavelength. At probe wavelength 365 and 450 nm the initial anisotropy is negative (parallel signal below the perpendicular signal), whereas it is positive at 408 and 600 nm. In all traces the anisotropy decays to zero after ~100 picoseconds (ps). At 365 nm, stimulated emission (SE) is expected to be observed, with an initial anisotropy very close to 0.4 [10]. Because a negative initial anisotropy is observed, the signal at this wavelength cannot only be attributed to SE. Excited-state absorption (ESA), with a much lower initial anisotropy, must also be present to explain the measured negative initial anisotropy at this probe wavelength. Note that the SE at 365 nm is most clearly observed in the parallel signal, and that this negative signal disappears together with the anisotropy. At 408 nm a short decay of ~1 ps is clearly present, followed by a slower decay on a nanosecond (ns) timescale. At 450 nm, the amount of SE is expected to be rather small (see below), and therefore the large initial negative anisotropy that is observed must mainly be attributed to ESA. Finally, at 600 nm, only ESA is expected to be present. A small positive anisotropy of the ESA can be observed.

4. Data analysis and discussion

First, the isotropic data are analyzed by a global analysis method [17,18]. The isotropic decay $I_{iso}(t)$ is described by a sum of exponential decays, each component having its own decay-associated difference spectrum (DADS) $A_i(\lambda)$ and concentration $c_i(t)$:

$$I_{iso}(t) = \left[\sum_{i=1}^{3} A_i(\lambda)_i \cdot c_i(t)\right] \otimes I(t) \quad (1)$$

$I(t)$ reflects the instrument response and $\otimes$ denotes convolution.

The concentration of each component is described by a mono-exponential decay:

$$c_i(t) = e^{-k_i t} \quad (2)$$

with k_i being the decay rate of component i.

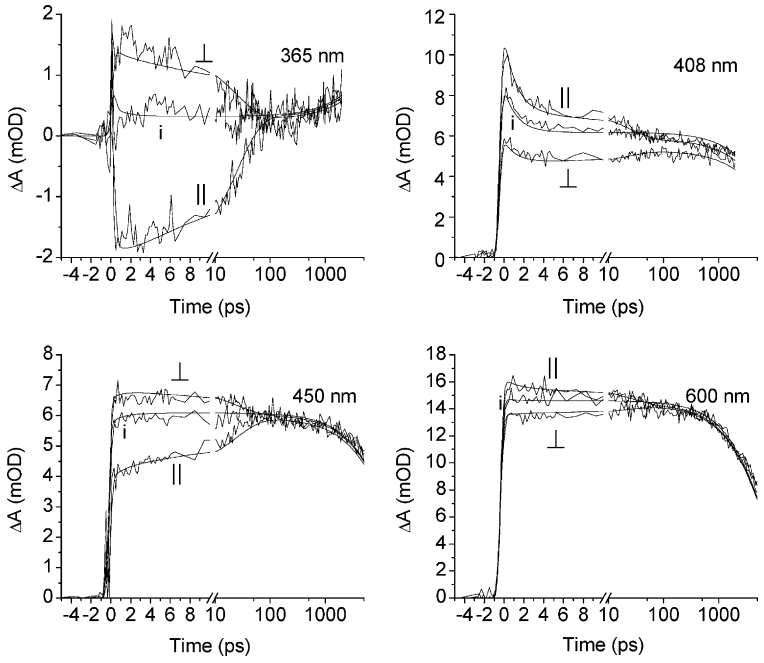

Fig. 1. Representative transient-absorption traces at different wavelengths. (||) Parallel signal; (*i*) isotropic signal; (⊥) perpendicular signal. Note that the time axis is linear up to 10 ps and logarithmic thereafter. Smooth lines: fit (see target analysis below).

The global analysis of the isotropic data (Eqs. (1) and (2)) resulted in three different lifetimes of 1.3 ps, 3.5 ns and ~14 ns, indicating structural heterogeneity of the sample. The decay-associated difference spectra (DADS) are shown in Fig. 2 (upper panel). The short-lived DADS (1.3 ps) shows ESA at ~400 and ~550 nm, and a negative feature centered at ~460 nm. It has to be noted that the negative features observed in the spectra can not be due to bleaching of the ground state of 2AP, because the lowest energy absorption band of 2AP peaks at 305 nm and the spectrum is zero above ~350 nm [10]. We therefore attribute this negative signal to SE, which is known to peak around 370 nm [7]. The second DADS (3.5 ns) shows ESA peaking at ~400 and ~530 nm, respectively, and some SE at ~430 nm. The third DADS (~14 ns) shows ESA peaking around 520 nm. The 3.5 ns DADS differs from the ~14 ns DADS by a larger contribution of SE superimposed upon the ESA in the former. The component decaying with 1.3 ps is ascribed to an unrelaxed state (see below) that decays into the 3.5 ns state most likely due to a reorganization of the surrounding solvent (spectral relaxation). The two ns components cannot be attributed to the earlier suggested 7-H and 9-H tautomeric states of 2AP (see below).

Secondly, both isotropic and anisotropic data were globally fitted using the following target analysis (see Fig. 3). The 2AP molecules are considered to be a heterogeneous mixture of 9-H tautomers having different interactions with the solvent. One population of 9-H tautomers interacts with the solvent in such a way that upon excitation a state is formed which rapidly transforms into a non-fluorescent long-lived state '1' (see below). Possibly, a proton transfer (which is too fast to be resolved with our setup) gives rise to rapid transformation of the excited 9-H tautomer into the non-fluorescent 7-H tautomer. However, transient-absorption experiments on 2AP-DNA dimers, for which the 7-H tautomer cannot exist because the 9 position of the base is involved in a covalent binding with deoxyribose, also reveal a similar long-lived non-fluorescent state (unpublished results). Therefore, it can be ruled out that the obtained non-fluorescent state originates from

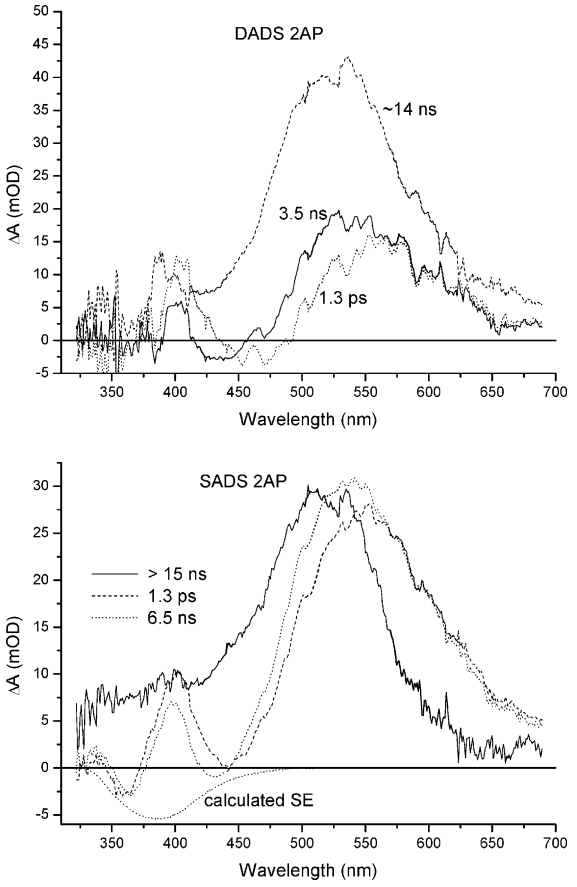

Fig. 2. Upper panel: DADS and their corresponding lifetimes as obtained from a global analysis of the isotropic transient-absorption data. Lower panel: SADS and their corresponding lifetimes as obtained from a target analysis of both the isotropic and polarized transient-absorption data. Negative black dotted line: calculated SE spectrum of 2AP (see text).

the 7-H tautomer, and we will therefore refer to this state as a 9-H 'dark' state. Parallel to this, there is another population of 9-H tautomers that interacts differently with the solvent and forms upon excitation a state (2) that is favorable to evolve into stabilized excited fluorescent 9-H tautomers (state 3).

The isotropic 1.3 ps DADS is interpreted as this transition from state 2 to 3. Evidence for heterogeneity of 2AP has already been given by the observation that the fluorescence quantum yield of 2AP is very dependent on the pH [14]. In all the traces, the anisotropy decays with ~25 ps, which is

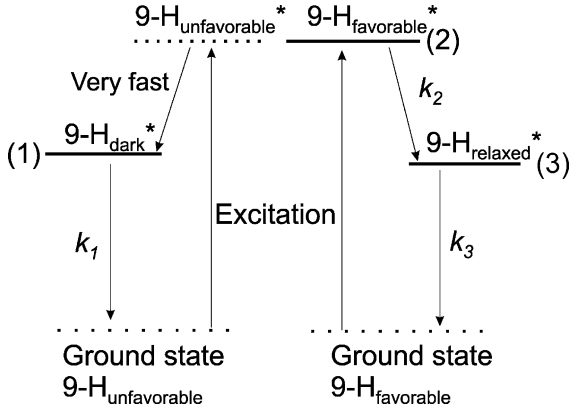

Fig. 3. Model used for fitting of the transient-absorption data, k_i are the fitted decay rates of the excited states.

in good agreement with earlier ultrafast fluorescence results [7]. To correctly fit the data one additional assumption was required concerning the anisotropy of the states involved. As can already be noticed from the 'raw' data, the anisotropy is very low in the visible part (where only ESA is expected), whereas it is much higher in the UV, where both SE and ESA take place (Fig. 1). To account for this wavelength dependent anisotropy behavior, we assume that the initial anisotropy of states 2 and 3 below 440 nm may be different from the initial anisotropy above 440 nm. The anisotropy of the long-lived state 1 was a single fitting parameter for the entire wavelength region. Using this target analysis, a good fit was obtained and the lifetimes and difference spectra of the different states with their corresponding anisotropies could be estimated. A schematic representation of the used target analysis is given in Fig. 3.

According to the model as depicted in Fig. 3, the following relations hold for the concentrations of the different states:

$$c_1(t) = c_1(0)\mathrm{e}^{-k_1 t}, \tag{3}$$

$$c_2(t) = c_2(0)\mathrm{e}^{-k_2 t}, \tag{4}$$

$$c_3(t) = \frac{k_2(\mathrm{e}^{-k_3 t} - \mathrm{e}^{-k_2 t})}{k_2 - k_3}. \tag{5}$$

The initial concentrations of states 1 and 2 were somewhat arbitrarily chosen in such a way that their corresponding spectra have approximately

the same maximum amplitude. Most likely, this is an oversimplification of reality (see below). The two polarized transient-absorption signals I_{par} and I_{perp} (parallel and perpendicular polarization of pump and probe light) were fitted to

$$\begin{bmatrix} I_{\text{par}}(t) \\ I_{\text{perp}}(t) \end{bmatrix} = \begin{bmatrix} \sum_{i=1}^{3} I_{\text{iso},i}(t) \cdot (1 + 2r_i(t)) \\ \sum_{i=1}^{3} I_{\text{iso},i}(t) \cdot (1 - r_i(t)) \end{bmatrix} \otimes I(t), \quad (6)$$

where $I_{\text{iso},i}(t)$ is the isotropic fluorescence signal of state i (as defined in Eq. (1), with corresponding concentrations as defined in Eqs. (3)–(5)), and $r_i(t)$ is its associated anisotropy.

The anisotropy r_i of component i is described as

$$r_i(t) = r_i(0)\mathrm{e}^{-t/\tau} \quad (7)$$

with $r_i(0)$ being the initial anisotropy of state i and τ the rotational correlation time, for which the same fitting parameter was used for all the different states. As explained above the initial anisotropy below 440 nm of states 2 and 3 was treated as an extra fitting parameter, and was allowed to be different from the initial anisotropy above 440 nm for these states. The initial anisotropy of state 1 was a single fitting parameter for the entire wavelength region.

To illustrate the quality of the fit an overview of several traces ranging from ~320 up to ~690 nm with the corresponding fits is given in Fig. 4. The obtained species associated difference spectra (SADS) are depicted in Fig. 2 (lower panel).

At time zero, two states (1 and 2) are present (Fig. 2 lower panel). State 1 shows a rather flat ESA profile over the whole wavelength region peaking around 520 nm and decays with a lifetime of >15 ns. The second state shows ESA peaking at both ~550 and ~400 nm and evolves with 1.3 ps into a new state (3) which decays with ~6.5 ns. It has to be noted that the total time window probed was 5 ns, and hence the precision of these 'long' times is low, which also explains differences in 'long' lifetimes that are obtained when using either the first (DADS) or the second model (SADS). A significant contribution of SE is observed around 370 nm for both states 2 and 3. It should be stressed that the spectral shape of the SE is obscured because of the ESA that is also present in this wavelength region. Therefore, the SE spectrum that was calculated from a measured steady-state emission spectrum of 2AP is also included in Fig. 2. The SE spectrum was calculated using the following relation [19]:

$$\left(\frac{\hbar\omega^3}{\pi^2 c^3}\right) B_{21} = A_{21} \quad (8)$$

with $\hbar$ Planck's constant, c the velocity of light, and B_{21} and A_{21} the Einstein coefficients describing SE and spontaneous emission, respectively. It should be noted that the SE will most likely show a dynamic Stokes shift which is reported to take place within 4 ps [20], comparable with the 1.3 ps time we find.

Interestingly, when state 2 evolves into 3 the ESA increases around ~500 nm while it goes down at ~400 nm. The difference between the 6.5 ns SADS and the 1.3 ps SADS is illustrated in Fig. 5.

Clearly, upon relaxation of state 2 into state 3, signal is gained around 500 nm while signal is lost around 400 nm. The gain in signal peaking at ~500 nm should most likely be attributed to a gain in ESA, because no significant SE is expected to be present around this wavelength. The loss in signal at ~400 nm can both be attributed to a loss of ESA and/or an increase of SE. Clearly, a large amount of reorganization takes place within 1.3 ps, which is not unexpected considering the large Stokes shift of ~5000 cm^{-1} between the lowest steady-state absorption band (305 nm) and the maximum of the steady-state emission (370 nm).

The anisotropy of state 1 is -0.2 ± 0.1. The anisotropy of state 2 and 3 in the 320–440 nm region is 0.35 ± 0.05, while above 440 nm it is 0.10 ± 0.02 and 0.08 ± 0.02, respectively. The concentration ratio of state 1 and state 2 is 0.3:0.7, indicating that the non-fluorescent state 1 is ~2.3 times less abundant than the fluorescent states 2 and 3. Considering the fact that the fluorescence quantum yield is 0.66 [10], practically no quenching should take place for the fluorescent subset of molecules (70% of all the molecules), which seems unlikely. The concentration ratio of states 1 and 2 (0.3:0.7) we obtain should therefore be considered as an upper limit.

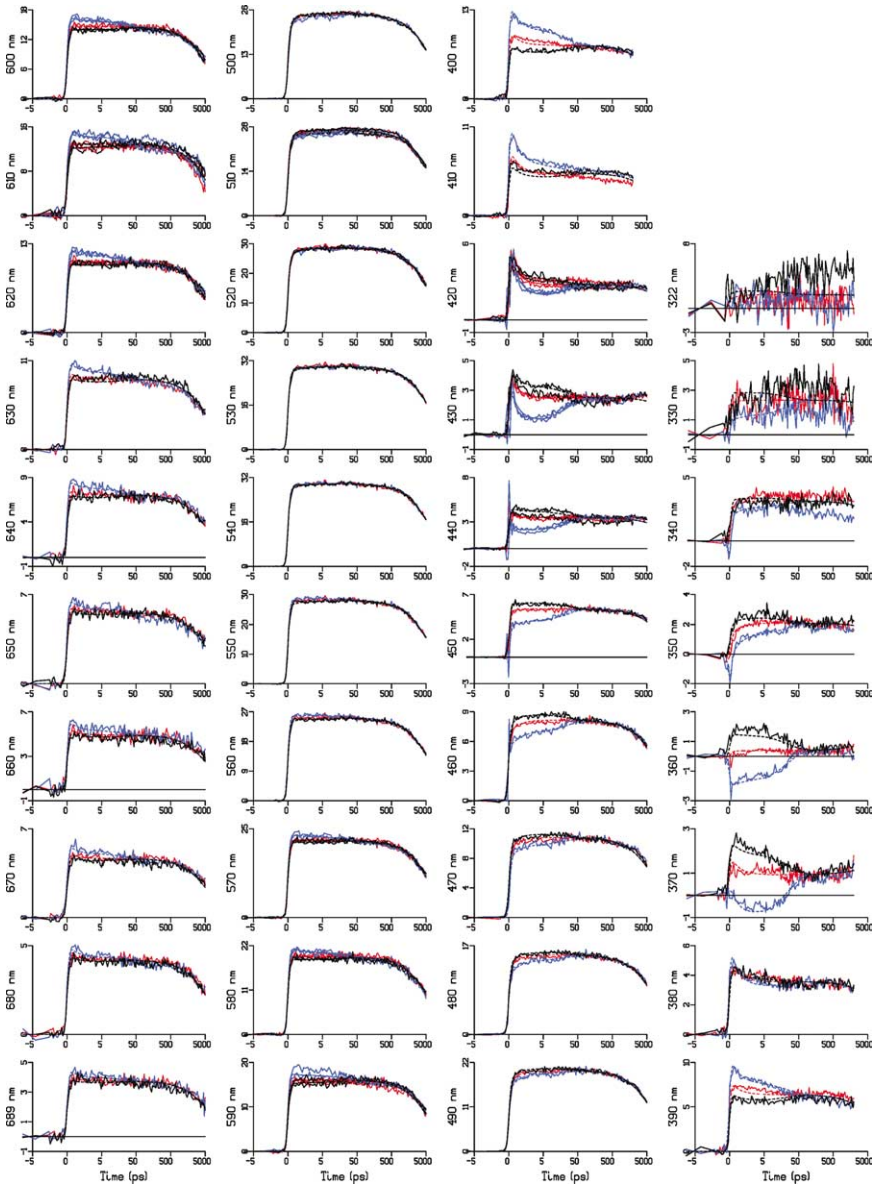

Fig. 4. Traces of both the isotropic and anisotropy data (mOD) with their corresponding fit at different wavelengths (vertical label). Blue, parallel signal; red, isotropic signal; black, perpendicular signal. Note that the time axis is linear up to 5 ps and logarithmic thereafter. Dashed lines: fit (target analysis). The data have been presented from ~320 nm (upper right panel) to ~690 nm (lower left panel), with intervals of 10 nm.

Summarizing, two different electronic states were revealed from the data. One state does show SE, whereas the other state does not. A clear relaxation is observed for the emitting state (reflected by the 1.3 ps lifetime), which can most likely be ascribed to spectral relaxation [20]. States 2 and 3 have ~0.35 anisotropy in the 320–440 nm range. The anisotropy of the SE is expected to have an anisotropy of 0.4, based on earlier steady-state measurements [10] and based on theory [21].

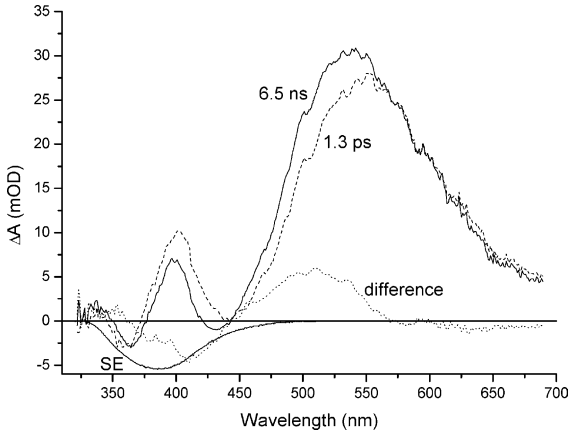

Fig. 5. Dashed, 1.3 ps SADS (state 2); line, 6.5 ns SADS (state 3); dotted, difference between SADS of state 3 and state 2; negative line, calculated SE spectrum.

Because the anisotropy in this wavelength region is both due to SE and ESA, it can be concluded that the ESA is also highly polarized up to 440 nm. In the 440–690 nm region, the polarization of the states 2 and 3 is very low ($\sim$0.1 and $\sim$0.08, respectively) indicating almost completely depolarized ESA. The -0.2 ± 0.1 anisotropy of state 1 indicates that the polarization of the ESA is perpendicular to the polarization of the ground-state absorption and illustrates the rather different electronic properties of the two states.

Acknowledgements

Dr. F. van Mourik, Institute of Condensed Matter Physics, University of Lausanne, and Dr. D.S. Larsen, Vrije Universiteit, are thanked for seminal contributions to the measurements.

References

[1] S. Wennmalm, L. Edman, R. Rigler, Proc. Natl. Acad. Sci. USA 94 (1997) 10641.
[2] J.-M.L. Pecourt, J. Peon, B. Kohler, J. Am. Chem. Soc. 123 (2001) 10370.
[3] C. Wan, T. Fiebig, S.O. Kelley, C.R. Treadway, J.K. Barton, A.H. Zewail, Proc. Natl. Acad. Sci. USA 96 (1999) 6014.
[4] F.D. Lewis, X. Liu, J. Liu, S.E. Miller, R.T. Hayes, M.R. Wasielewski, Nature 406 (2000) 51.
[5] C.R. Cantor, P.R. Schimmel, Biophysical Chemistry Part 2., W.H. Freeman and Company, New York, 1980.
[6] T.M. Nordlund, D. Xu, K.O. Evans, Biochemistry 32 (1993) 12090.
[7] O.F.A. Larsen, I.H.M. van Stokkum, B. Gobets, R. van Grondelle, H. van Amerongen, Biophys. J. 81 (2001) 1115.
[8] S.O. Kelley, J.K. Barton, Science 283 (1999) 375.
[9] V. Shafirovich, A. Dourandin, W. Huang, N.P. Luneva, N.E. Geacintov, Phys. Chem. Chem. Phys. 2 (2000) 4399.
[10] A. Holmén, B. Nordén, B. Albinsson, J. Am. Chem. Soc. 119 (1997) 3114.
[11] L.C. Sowers, G.V. Fazakerley, R. Eritja, B.E. Kaplan, M.F. Goodman, Proc. Natl. Acad. Sci. USA 83 (1986) 5434.
[12] A. Broo, A. Holmén, Chem. Phys. 211 (1996) 147.
[13] A. Broo, J. Phys. Chem. A 102 (1998) 526.
[14] C. Santosh, P.C. Mishra, Spectrochim. Acta 47A (1991) 1685.
[15] C.C. Gradinaru, I.H.M. van Stokkum, A.A. Pascal, R. van Grondelle, H. van Amerongen, J. Phys. Chem. B 104 (2000) 9330.
[16] V. Shafirovich, A. Dourandin, W. Huang, N.P. Luneva, N.E. Geacintov, J. Phys. Chem. B 103 (1999) 10924.
[17] I.H.M. van Stokkum, T. Scherer, A.M. Brouwer, J.W. Verhoeven, J. Phys. Chem. 98 (1994) 852.
[18] A.R. Holzwarth, in: J. Amesz, J. Hoff (Eds.), Biophysical Techniques in Photosynthesis, Kluwer Academic Publishers, Dordrecht, 1996, p. 75.
[19] R. Loudon, The Quantum Theory of Light, Oxford University Press, New York, 1991.
[20] S.K. Pal, J. Peon, A.H. Zewail, Chem. Phys. Lett. 363 (2002) 57.
[21] H. van Amerongen, W.S. Struve, Meth. Enzymol. 246 (1995) 259.